



Compositional Modification of Epitaxial Pb(Zr,Ti)O₃ Thin Films for High-Performance Piezoelectric Energy Harvesters

Kweon, Sang Hyo

Kim, Eun-Ji

Tan, Goon

Kanno, Isaku

(Citation)

Advanced Materials Interfaces, 11(2):2300634

(Issue Date)

2024-01-16

(Resource Type)

journal article

(Version)

Version of Record

(Rights)

© 2023 The Authors. Advanced Materials Interfaces published by Wiley-VCH GmbH
This is an open access article under the terms of the Creative Commons Attribution License, which permits use, distribution and reproduction in any medium, provided the original work is properly cited.

(URL)

<https://hdl.handle.net/20.500.14094/0100486179>



Compositional Modification of Epitaxial Pb(Zr,Ti)O₃ Thin Films for High-Performance Piezoelectric Energy Harvesters

Sang Hyo Kweon, Eun-Ji Kim, Goon Tan, and Isaku Kanno*

In this study, Piezoelectric energy harvesters (PEHs) are fabricated based on epitaxial Pb(Zr,Ti)O₃ (PZT) thin films deposited by an RF magnetron sputtering with varied Zr/[Zr+Ti] ratio. For a compatibility with micro-electromechanical systems, the epitaxial PZT thin films are deposited on Si substrates (PZT/Si). The morphotropic phase boundary (MPB) are formed in the compositional range of $0.44 \leq \text{Zr}/[\text{Zr}+\text{Ti}] \leq 0.51$ of the epitaxial PZT/Si, which is far broader than that of the bulk PZT. Meanwhile, effective transverse piezoelectric coefficient ($|e_{31,f}|$) values are evaluated by the direct and converse piezoelectric effects using the unimorph cantilever method. Among the compositions, the rhombohedral-dominant MPB (MPB-R) of $\text{Zr}/[\text{Zr}+\text{Ti}] = 0.51$ exhibits a direct $|e_{31,f}|$ of 10.1 C m^{-2} and a relative permittivity (ϵ_r) of 285, leading to the maximum figure of merit of 40 GPa in this study. On the other hand, the maximum converse $|e_{31,f}|$ of 14.0 C m^{-2} is measured from the tetragonal-dominant MPB (MPB-T) of $\text{Zr}/[\text{Zr}+\text{Ti}] = 0.44$. At a resonance frequency, the MPB-T presents a high output power density of $301.5 \mu\text{W}^{-1}/(\text{cm}^2 \text{ g}^2)$ under an acceleration of $3 \text{ m}^{-1} \text{ s}^{-2}$, which is very promising for the high-performance PEH applications.

have been persistently investigated for the use as a semi-permanent power source of electronic devices.^[7–11] For instance, PEHs can be incorporated in electronics located at remote and dangerous places where a recharging of battery is quite difficult, in wireless-communication modules that suffer from a battery problem that lots of sensors would cause, and in wearable devices for health care systems without batteries.^[11,12] Yet, to catch up with the increasing electrical power requirements for an operation of those devices, it became necessary to integrate PEHs that have far better performances. In this context, a criterion for the comparison of PEHs' performances was needed, and the figure of merit (FOM) has been claimed as follows;^[13,14]

$$FOM = \frac{(|e_{31,f}|)^2}{\epsilon_0 \epsilon_r} \quad (1)$$

1. Introduction

Pb(Zr,Ti)O₃ (PZT) thin films have been exploited for a wide span of applications owing to their good piezoelectric properties.^[1–7] Among the applications, piezoelectric energy harvesters (PEHs)

where $|e_{31,f}|$, ϵ_r , and ϵ_0 are the effective transverse piezoelectric coefficient, the relative permittivity of piezoelectric material, and the vacuum permittivity, respectively. Here, note that the $|e_{31,f}|$ should be obtained under the occurrence of the direct piezoelectric effect by which the operation of PEHs are governed.

According to the Equation (1), it is preferable to use a PZT thin film with a large direct $|e_{31,f}|$ and a low ϵ_r to increase the FOM. The simplest way to achieve this in terms of material design is to modify the composition of the PZT thin film. Typically, the morphotropic phase boundary (MPB) composition has been a major concern due to better piezoelectric performances than other compositions.^[15,16] Interestingly, the MPB composition of bulk ceramics, i.e., Pb(Zr_{0.52}Ti_{0.48})O₃ did not guarantee a superior $|e_{31,f}|$ value when the PZT was made into a thin film, though. The maximum value of $|e_{31,f}|$ was acquired over a broad compositional range of $0.40 \leq \text{Zr}/[\text{Zr}+\text{Ti}] \leq 0.55$, being influenced by factors such as microstructures, preferred orientations, deposition processes, substrate materials, and besides, the type of piezoelectric effect exploited for evaluation.^[17–22] This implies that it is crucial to refrain from generalizing the selection of compositions. Moreover, epitaxial growth of PZT thin films were greatly effective for optimizing piezoelectric responses owing to the films' anisotropic nature.^[8,23] Particularly, [001]-oriented epitaxial growth was favorable for a low ϵ_r , leading to a large FOM.^[24] Based on the above, it can be concluded that PZT thin films

S. H. Kweon, I. Kanno
Department of Mechanical Engineering
Kobe University
1-1 Rokkodai-cho, Nada-ku, Kobe 657-8501, Japan
E-mail: kanno@mech.kobe-u.ac.jp

E.-J. Kim
Department of Materials Science and Engineering
Korea University
145 Anam-ro, Seongbuk-gu, Seoul 02841, South Korea
G. Tan
Division of Physics Faculty of Liberal Arts
Sciences and Global Education
Osaka Metropolitan University
1-1 Gakuen-cho, Naka-ku, Osaka, Sakai 599-8531, Japan

The ORCID identification number(s) for the author(s) of this article can be found under <https://doi.org/10.1002/admi.202300634>

© 2023 The Authors. Advanced Materials Interfaces published by Wiley-VCH GmbH. This is an open access article under the terms of the Creative Commons Attribution License, which permits use, distribution and reproduction in any medium, provided the original work is properly cited.

DOI: 10.1002/admi.202300634

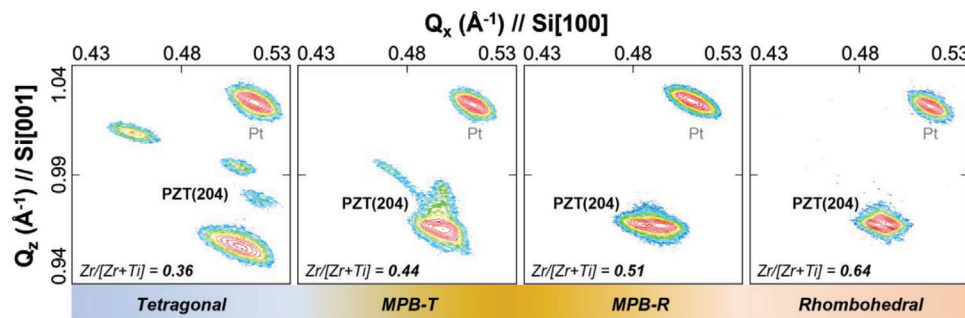


Figure 1. RSM images of epitaxial PZT/Si with various PZT compositions of $Zr/[Zr+Ti] = 0.36, 0.44, 0.51$, and 0.64 . The images were taken in the vicinity of the $PZT(204)_{pc}$ node within the reciprocal lattice.

should be prepared with modified compositions and grown epitaxially for high-performance PEHs.

Meanwhile, so as to fabricate PEHs into more sophisticated and miniaturized architectures, micro-electromechanical systems (MEMS) technique is strongly desired.^[23–27] As a matter of fact, for a facile deposition of the epitaxial PZT thin films, single-crystal substrates such as MgO and SrTiO₃ are typically used because of small lattice mismatches of <5% against PZT.^[28–32] However, Si substrate is the most compatible with conventional MEMS technique. Hence, investigations on PEHs that were fabricated from epitaxially grown PZT thin films on Si substrates (PZT/Si) have been implemented.^[24,33,34] In particular, a micro-cantilever fabricated from an epitaxial PZT of $Zr/[Zr+Ti] = 0.8$ thin film demonstrated an excellent output power density of $560 \mu W^{-1} (cm^{-2} g^{-2})$ (where g denotes an gravitational acceleration, $1 g = 9.8 m s^{-2}$) owing to a large *FOM* of ≈ 28 GPa.^[24,33] In spite of such a high output performance, it is a bit open to question whether the PZT composition is an optimized one, as PZT thin films exhibited the highest *FOM* at the vicinity of conventional MPB in several cases.^[17,18] Especially, PZT of $Zr/[Zr+Ti] = 0.52$ on MgO substrates possessed the highest *FOM* of 40 GPa within a series of PZT compositions,^[18] which is superior to the value above. In this sense, it is essential to reevaluate the compositional dependence of *FOM* for epitaxial PZT/Si, utilizing a reliable evaluation approach.

In this study, we fabricated the epitaxial PZT/Si into unimorph cantilevers with various PZT compositions. The direct and converse $|e_{31,f}|$ was evaluated, revealing that the optimal composition varied depending on the type of piezoelectric effect. Output performances of the PEHs were evaluated as well. It should be emphasized that the evaluation methodology for the output performance is exactly the same as that for the *FOM* measured by the direct piezoelectric effect,^[34] allowing for an authentic correlation between them to be explored.

2. Results and Discussion

2.1. Crystal Structures of Epitaxial PZT/Si

Figure S1 (Supporting Information) displays out-of-plane X-ray diffraction (XRD) patterns of the epitaxial PZT thin films that were prepared for this study. Diffraction peaks assigned to $(00l)_{pc}$ (the subscript *pc* denotes pseudocubic coordinates) crystallographic planes are observed, suggesting that the PZT was grown

with a preferred orientation. For a detailed insight for the crystal structure of the PZT, reciprocal space mapping (RSM) images around the $PZT(204)_{pc}$ node in the reciprocal lattice were taken, as shown in **Figure 1**. A big spot accompanied by three small spots was clearly observed from the PZT of $Zr/[Zr+Ti] = 0.36$, which is a typical pattern of the Ti-rich epitaxial PZT thin films with a tetragonal structure.^[34,35] Lattice parameters were calculated as $a = 0.3992$ nm and $c = 0.4177$ nm from the big spot that indicates *c*-domain of the tetragonal PZT. On the other hand, the PZT of $Zr/[Zr+Ti] = 0.64$ had explicitly distinguishable two spots side by side. This pattern is considered being originated from a rhombohedral twin structure that has been usually observed from Zr-rich PZT and BiFeO₃ epitaxial thin films.^[36–39] When it comes to $Zr/[Zr+Ti] = 0.44$ and 0.51 , the co-existence of tetragonal and rhombohedral phases was disclosed by out-of-plane XRD patterns obtained by synchrotron radiation XRD (SR-XRD). Diffraction patterns for (004) plane of PZT were comprised of several peaks that correspond to the tetragonal and rhombohedral phases. In case of the PZT of $Zr/[Zr+Ti] = 0.44$, the ratio of the tetragonal phase was dominant (MPB-T, Figure S2a, Supporting Information), while the rhombohedral phase mainly consisted of the $Zr/[Zr+Ti] = 0.51$ (MPB-R, Figure S2b, Supporting Information). It deserves attention that even though the tetragonal phase existed, very little amounts of *a*-domains were identified in the MPB-R. From the above, the composition range for the MPB was found to be quite broad compared to that of bulk PZT materials. Commonly, the crystal structure of epitaxial thin films exhibits a distinct behavior in response to compositional variations.^[40,41] This can be attributed to the lattice constraints exerted by substrates, which induce strong internal stress within the PZT material.

2.2. Electrical Properties of Epitaxial PZT/Si

Ferroelectric properties of the epitaxial PZT thin films are shown in **Figure 2**. Rectangular-like polarization-electric field (*P*–*E*) hysteresis curves were obtained from the tetragonal and the MPB-T PZT, indicating that a swift reversal of *c*-domains and fast 90° domain-wall motion occurred upon applying electric fields exceeding coercive electric field (*E_c*). In contrast, PZT with the rhombohedral phase exhibited a progressive polarization change, which is attributed to rotation and alignment of $\langle 111 \rangle_{pc}$ domains. Also, the saturation polarization (*P_s*) decreased in a

large extent because dipole moments were not aligned to the measurement direction. In case of the MPB-R, meanwhile, a hysteresis shape similar to that of the tetragonal and MPB-T was obtained although the rhombohedral phase was dominant. The exact reason for this phenomenon remains unclear, yet it is probable that domains were predominantly oriented toward the $[001]_{\text{pc}}$ direction owing to the very small interaxial angle γ in the rhombohedral symmetry. Incidentally, the hysteresis curves are shifted toward the positive side throughout the whole compositions, implying that the upward polarization is stable within the epitaxial PZT thin films. This also let us know the suitable poling direction, i.e., a negative bias on the top electrodes.

Figure 3 illustrates direct and converse $|e_{31,f}|$ values of epitaxial PZT/Si cantilevers with various PZT compositions, while the dimensions of each cantilever are offered in Table S1 (Supporting Information). The direct $|e_{31,f}|$ values along with output voltages (V_{out}) are plotted as a function of vibrational acceleration in Figure 3a. In a cantilever, the V_{out} increased proportionally with the acceleration, leading to the almost constant $|e_{31,f}|$ irrespective of the acceleration value. It is notable, that the cantilevers could endure the acceleration of up to $9 \text{ m}^{-1} \text{ s}^{-2}$, retaining their piezoelectric responses. In addition, it was obvious that the direct $|e_{31,f}|$ values became larger when the composition of PZT was located at the region of MPB. Within the MPB, we could observe that the MPB-R manifested the maximum direct $|e_{31,f}|$ of 10.1 C m^{-2} . The relatively smaller direct $|e_{31,f}|$ of 9.4 C m^{-2} was obtained from the MPB-T, which can be attributed to the existence of a nonnegligible amount of the a -domains that has a piezoelectric behavior opposite to that of the c -domains under the 31-mode operation. In Figure 3b, the converse $|e_{31,f}|$ values along with output tip displacements (δ_{out}) are exhibited. Interestingly, the maximum converse $|e_{31,f}|$ of 14.0 C m^{-2} was yielded from the MPB-T, revealing that the compositions for the maximum direct and converse $|e_{31,f}|$ values were not necessarily identical. This is because the converse $|e_{31,f}|$ value incorporates extrinsic contributions that arise from the 90° domain-wall motion. From the above findings, the epitaxial PZT/Si serves as a compelling example that highlights the importance of distinguishing between the direct and converse $|e_{31,f}|$ when evaluating piezoelectric devices.

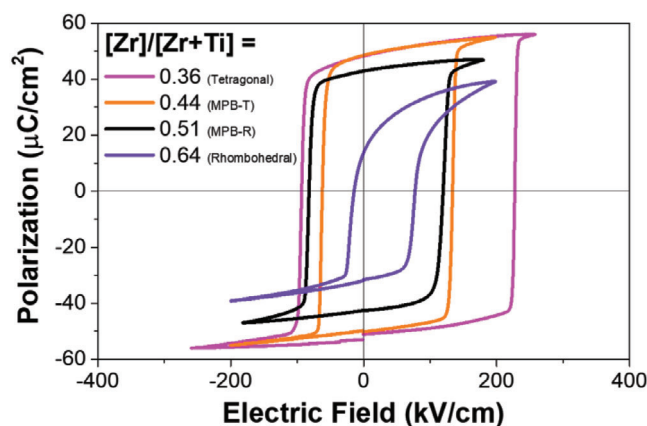


Figure 2. P - E hysteresis curves of epitaxial PZT/Si.

2.3. Output Performance of PEH and its Relationship with Direct FOM

Output performances of the cantilever-type PEH are shown in Figure 4. It should be noted that they were tested on the basis of the same evaluation methodology applied for the measurement of direct $|e_{31,f}|$. The only thing we regulated was the load resistance (R_L) value. The R_L dependence of output power (P_{out}) for various PZT compositions are depicted in Figure 4a. The epitaxial PZT/Si cantilever with the MPB-R produced an unrivaled P_{out} of 14.5

μW when tested under the R_L of $10 \text{ k}\Omega$. For all the PZT compositions covered in this study, Figure S3 (Supporting Information) provides the P_{out} and V_{out} corresponding to different values of R_L . Moreover, the influences of acceleration on the P_{out} and resonance frequency (f_r) of the MPB-R cantilever were investigated by fixing the R_L as $10 \text{ k}\Omega$, as shown in Figure 4b. It seems like that even when subjected to high acceleration over the 1 g ($9.8 \text{ m}^{-1} \text{ s}^{-2}$), the cantilever did not suffer significant damage. Otherwise, the experimental result would have been greatly deviated from the theoretical values that were derived following previous studies.^[34,42] This result is consistent with the nearly constant $|e_{31,f}|$ observed in terms of the acceleration (Figure 3a). Furthermore, we observed that the f_r decreased from 427 to 421 Hz as the acceleration was raised, which is a trend very similar to what we observed in our previous studies.^[34,42] This can be attributed to the nonlinear stiffness resulting from the geometric deformation of PEHs during vibration.^[11]

Figure 5 describes direct FOMs that were derived using Equation (1), along with the corresponding output power densities. Figure 5a illustrates how the direct FOMs and output power densities depend on the PZT composition. The trend of FOM was very similar to that of direct $|e_{31,f}|$ in Figure 3a, with the MPB-R achieving the highest FOM of 40 GPa . This is the highest value ever reported for the PZT thin films deposited on Si substrates owing to the large direct $|e_{31,f}|$ and low ϵ_r . On top of that, the maximum output power density of $301.5 \mu\text{W}^{-1} (\text{cm}^{-2} \text{ g}^{-2})$ was acquired at the same MPB-R composition, when the acceleration was $3 \text{ m}^{-1} \text{ s}^{-2}$. Meanwhile, although it is generally accepted that a high FOM ensures a large output power density, it is important to emphasize that experimentally demonstrating this correlation can be quite challenging.^[43] Nonetheless, it is noteworthy that variation in output power density closely paralleled the changes in FOM values, as depicted in Figure 5a. When the output power densities are plotted with respect to the FOMs, a linear relationship emerged, as shown in Figure 5b. This became possible by employing the same evaluation methodology for the FOM and output performance, highlighting the effectiveness of our approach in evaluating the performance of cantilever-type PEHs.

3. Conclusion

This study investigated the compositional dependence of crystal structure and piezoelectric properties of epitaxial PZT/Si cantilevers. XRD patterns and RSM images revealed an epitaxial growth along the $[001]_{\text{pc}}$ direction of the PZT crystal. As the $\text{Zr}/[\text{Zr}+\text{Ti}]$ increased, the phase of PZT was transformed from the tetragonal to the rhombohedral phase. MPB was found within a broad composition range of $0.44 \leq \text{Zr}/[\text{Zr}+\text{Ti}] \leq 0.51$, which was

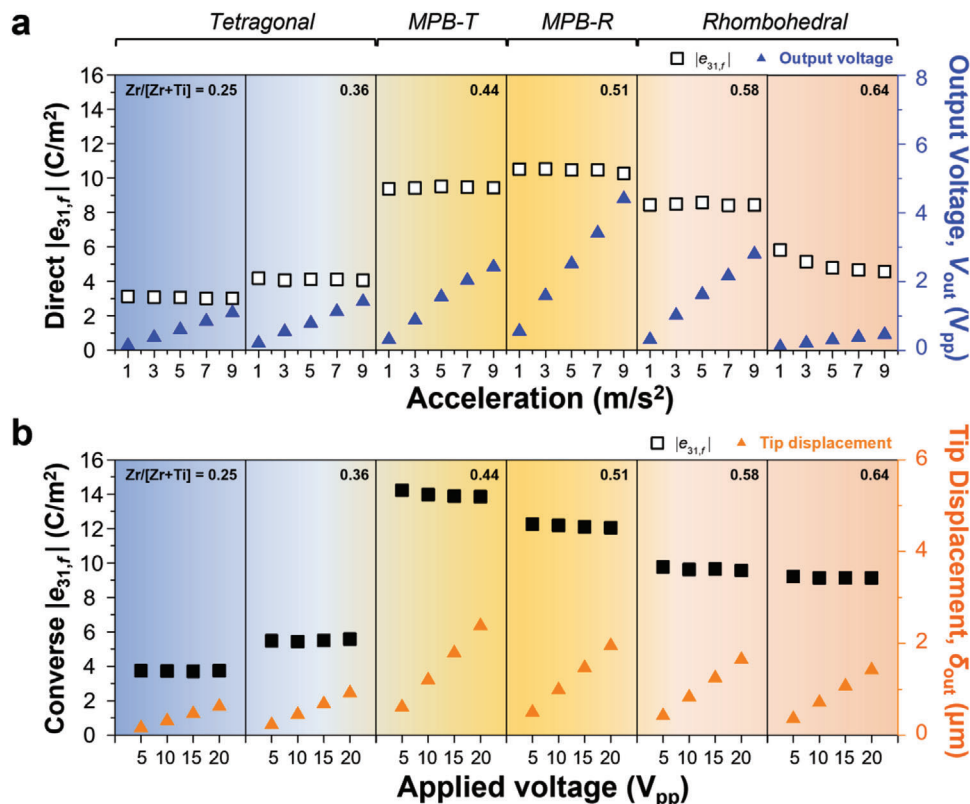


Figure 3. a) Direct $|e_{31,f}|$ and V_{out} versus acceleration and b) converse $|e_{31,f}|$ and δ_{out} versus applied voltage of epitaxial PZT/Si cantilevers with various compositions.

fairly different from the behavior of bulk ceramics. P - E hysteresis curves showed different polarization behaviors depending on the crystal structure, with the tetragonal, MPB-T and MPB-R phases exhibiting a swift reversal, while the rhombohedral phase exhibited progressive polarization change. Direct and converse $|e_{31,f}|$ of the epitaxial PZT/Si cantilevers was evaluated and observed to be larger in compositions located at the MPB region. Especially,

the MPB-R showed the maximum of 10.1 C m^{-2} , resulting in the FOM of 40 GPa that is the largest reported to date for epitaxial PZT/Si. The maximum converse $|e_{31,f}|$ was measured from the MPB-T with an average value of 14.0 C m^{-2} . It is worth noticing that the maximum $|e_{31,f}|$ was different depending on the type of piezoelectric effect. Output performances of the epitaxial PZT/Si cantilevers were examined, as well. The MPB-R generated the

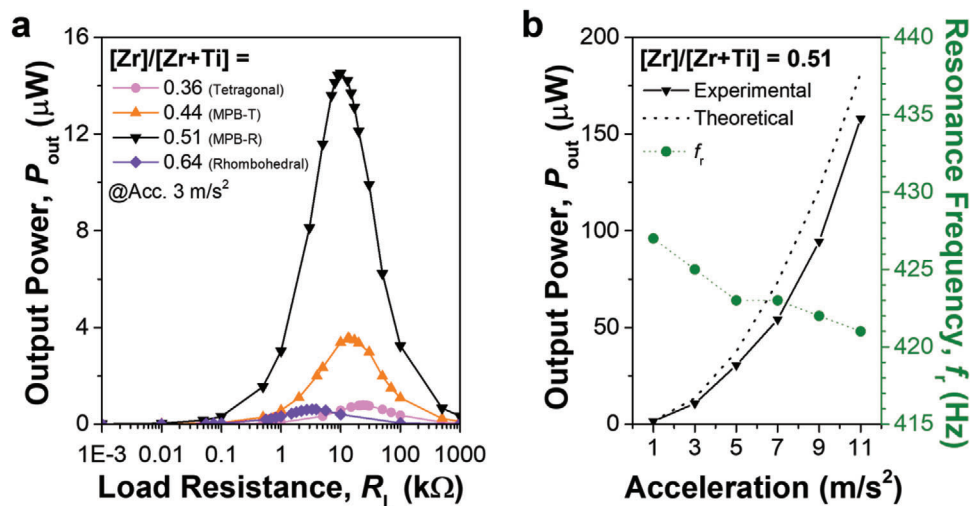


Figure 4. a) P_{out} versus R_L acquired from epitaxial PZT/Si PEHs with various compositions. Acceleration was set at a constant value of $3 \text{ m}^{-1} \text{ s}^{-2}$. b) P_{out} and f_r versus acceleration obtained from the epitaxial PZT/Si PEH with the MPB-R. R_L was set at a constant value of $10 \text{ k}\Omega$.

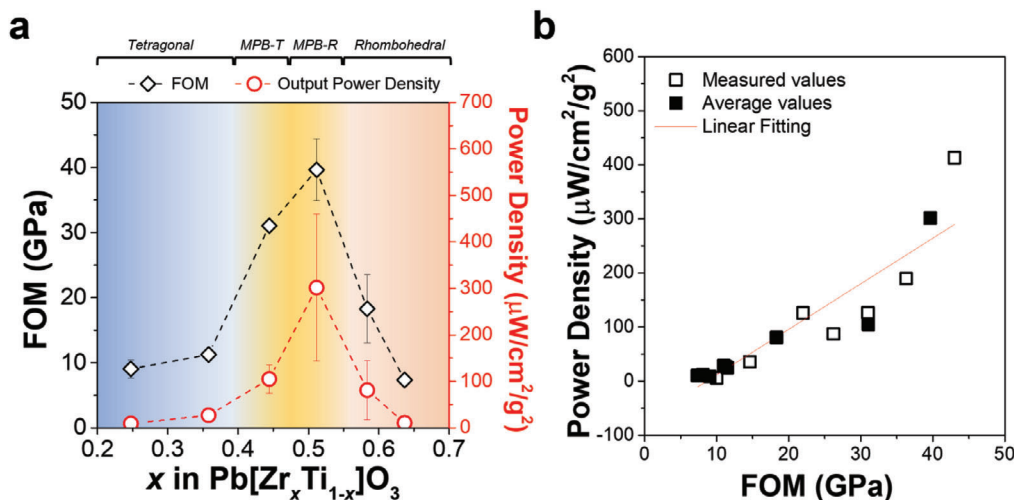


Figure 5. a) FOMs and output power densities versus PZT composition. Error bars for the experimental standard deviation are presented, as well. b) A relationship between the output power densities and FOMs; white and black squares indicate measured and average values, respectively. The average values correspond to the data points in (a).

maximum P_{out} of $14.5 \mu\text{W}$ when the circuit was attached with the R_L of $10 \text{ k}\Omega$ and the acceleration was $3 \text{ m}^{-1} \text{ s}^{-2}$. At that point, the output power density was calculated to be $301.5 \mu\text{W}^{-1} (\text{cm}^{-2} \text{ g}^{-2})$. In summary, we could make an epitaxial PZT/Si with an excellent FOM, therefore, a high-performance PEH could be realized. Moreover, we suggested a linear relationship between FOM and output power density, which demonstrates the validity of the approach we used.

4. Experimental Section

Fabrication of Cantilever-Shape Unimorph PEHs: Epitaxial PZT thin films with a thickness range of $2\text{--}3 \mu\text{m}$ were deposited on (001)SrRuO₃ (40 nm)/(100)Pt (150 nm)/ZrO₂ (50 nm)-coated Si substrate (725 μm) that was purchased from KRYSTAL Inc., with a size of $2 \times 2 \text{ cm}^2$ by an RF magnetron sputtering. The key factor for the epitaxial growth of PZT thin films was the epitaxial growth of Pt bottom electrode. Previous studies have revealed that the use of a Y-doped ZrO₂ buffer layer facilitates the epitaxial growth of Pt on Si substrates.^[44,45] Meanwhile, the Zr/[Zr+Ti] ratio of the thin films was manipulated by utilizing commercially available 3-inch sputtering targets of predetermined compositions TOSHIMA, $\text{Pb}(\text{Zr}_{0.30}\text{Ti}_{0.70})\text{O}_3$, $\text{Pb}(\text{Zr}_{0.53}\text{Ti}_{0.47})\text{O}_3$, $\text{Pb}(\text{Zr}_{0.58}\text{Ti}_{0.42})\text{O}_3$, and $\text{Pb}(\text{Zr}_{0.70}\text{Ti}_{0.30})\text{O}_3$, as well as a combination of them. To compensate evaporations of Pb elements during the deposition, excess PbO was added to the targets. The deposition of epitaxial PZT thin films followed the procedures outlined in our previous studies.^[2,28] During the sputtering with an RF power of 90 W, the substrate temperature was maintained as 660°C . The sputtering chamber was filled with a mixed gas of $\text{Ar}/\text{O}_2 = 19.5/0.5 \text{ sccm}$ under a working pressure of 0.5 Pa. The PZT/Si was diced into a cantilever shape after the 80 nm-thick Pt top electrode layer was formed by the sputtering. The length and the width of the cantilevers were aimed as ≈ 14 and 2 mm, respectively.

Structural and Dielectric/Ferroelectric Properties of PZT Thin Film: A high-resolution XRD (HR-XRD, RIGAKU, SmartLab) equipped with a four-axis diffractometer was used to assess the crystal structure of the epitaxial PZT thin films, utilizing CuK α radiation ($\lambda = 1.54 \text{ \AA}$) at 40 kV and 30 mA. Detailed analyses were conducted by RSM images. In addition, SR-XRD was utilized to precisely evaluate crystal structures. Monochromatic X-rays

(12.4 keV, $\lambda = 1.0 \text{ \AA}$) were irradiated to the thin films at the synchrotron radiation facility SPring-8, beamline BL46XU.

To measure dielectric and ferroelectric properties, round-shaped Pt top electrodes were formed on PZT thin films by means of sputtering. ϵ_r and dielectric loss ($\tan \delta$) were measured at 1 kHz using an LCR meter (HIOKI, IM3536). Room-temperature P - E curves were taken by a ferroelectric tester (RADIANT Technologies, Precision Multiferroic II).

Evaluation of Piezoelectric Properties and PEH Output Performance: The piezoelectric properties, encompassing both direct and converse piezoelectric effects of the epitaxial PZT/Si, were assessed adopting the unimorph cantilever method, which was described in our earlier studies.^[31,34] The direct $|e_{31,f}|$ and PEH performances were characterized using the direct piezoelectric effect. A 0.96 g tungsten block as a proof mass was attached to the tip of the epitaxial PZT/Si cantilever. All the examined cantilevers were firmly fixed to clamping jig with a 5 cN m torque to prevent the movement of f_r during the measurement. Prior to an operation of the PZT/Si cantilevers, a negative unipolar oscillation (1000 Hz, $-20 \text{ V}_{\text{pp}}$) was applied to the top electrode for 1 min as a poling treatment using a function generator (NF Corporation, WF1943B) with an add-on power amplifier (NF Electronic Instruments, 4015). The cantilever was vibrated by a shaker equipped with an accelerometer and input tip displacements (δ_{in}) were estimated by electric signal extracted from a laser Doppler vibrometer (ONOSOKKI, LV-1720A). During the vibration, a frequency response analyzer is used (NF Corporation, FRA5095) to check the f_r . V_{out} was measured using an oscilloscope (NF Corporation, GDS1062A) under various R_L ranging from 10^{-1} to $10^6 \Omega$. To calculate the direct $|e_{31,f}|$, the relationship was employed between δ_{in} and V_{out} , which was amplified in our previous study.^[34] From the direct $|e_{31,f}|$ alongside the ϵ_r obtained from the cantilever, the direct FOM was calculated according to the Equation (1). P_{out} was calculated as V_{out}^2/R_L .

The converse $|e_{31,f}|$ was characterized using the converse piezoelectric effect. A negative unipolar sinusoidal oscillation was applied to the top electrode of the epitaxial PZT/Si cantilever using a function generator (NF Corporation, WF1946A), while the bottom electrode was grounded. The applied voltage was adjusted within the range of $-5 \text{--} -20 \text{ V}_{\text{pp}}$ at a frequency of 600 Hz, far lower than the resonance frequency during the measurement of converse piezoelectricity, which was $\approx 2.3 \text{ kHz}$. The δ_{out} was measured using a laser Doppler vibrometer (Demodulator AT3700, GRAPHTEC, and Japan) and a digital oscilloscope (LT344, LeCroy, USA). To calculate the converse $|e_{31,f}|$, the relationship was utilized between the applied voltage and δ_{out} , as discussed in our previous studies.^[31,34]

Supporting Information

Supporting Information is available from the Wiley Online Library or from the author.

Acknowledgements

This work was supported by the JST-CREST (grant no. JPMJCR20Q2).

Conflict of Interest

The authors declare no conflict of interest.

Data Availability Statement

The data that support the findings of this study are available from the corresponding author upon reasonable request.

Keywords

epitaxial growth, piezoelectric energy harvesters, PZT composition, Si substrates, transverse piezoelectricity

Received: July 31, 2023

Revised: October 3, 2023

Published online: October 27, 2023

- [1] N. Izyumskaya, Y. I. Alivov, S. J. Cho, H. Morkoç, H. Lee, Y. S. Kang, *Crit. Rev. Solid State Mater. Sci.* **2007**, 32, 111.
- [2] I. Kanno, H. Kotera, K. Wasa, *Sens. Actuators, A* **2003**, 107, 68.
- [3] P. Muralt, *IEEE Trans. Ultrason. Ferroelectr. Freq. Control* **2000**, 47, 903.
- [4] P. Muralt, N. Ledermann, J. Paborowski, A. Barzegar, S. Gentil, B. Belgacem, S. Petitgrand, A. Bosseboeuf, N. Setter, *Ultrason. Ferroelectr. Freq. Control* **2005**, 52, 2276.
- [5] K.-I. Park, J. H. Son, G. T. Hwang, C. K. Jeong, J. Ryu, M. Koo, I. Choi, S. H. Lee, M. Byun, Z. L. Wang, K. J. Lee, *Adv. Mater.* **2014**, 26, 2514.
- [6] K. Ueda, S. H. Kweon, H. Hida, Y. Mukouyama, I. Kanno, *Sens. Actuators, A* **2021**, 327, 112786.
- [7] R. Harada, N. Iwamoto, S. H. Kweon, T. Umegaki, I. Kanno, *Sens. Actuators, A* **2021**, 322, 112617.
- [8] S. Priya, H. C. Song, Y. Zhou, R. Varghese, A. Chopra, S. G. Kim, I. Kanno, L. Wu, D. S. Ha, J. Ryu, R. G. Polcawich, *Energy Harvest. Syst.* **2017**, 4, 3.
- [9] H. Liu, J. Zhong, C. Lee, S. W. Lee, L. Lin, *Appl. Phys. Rev.* **2018**, 5, 041306.
- [10] H. C. Song, S. W. Kim, H. S. Kim, D. G. Lee, C. Y. Kang, S. Nahm, *Adv. Mater.* **2020**, 32, 2002208.
- [11] H. Liang, G. Hao, O. Z. Olszewski, *Sens. Actuators, A* **2021**, 331, 112743.
- [12] M. Safaei, H. A. Sodano, S. R. Anton, *Smart Mater. Struct.* **2019**, 28, 113001.
- [13] R. Xu, S. G. Kim, *presented at PowerMEMS 2012, December, Atlanta, GA, USA*, **2012**.
- [14] S. H. Baek, J. Park, D. M. Kim, V. A. Aksyuk, R. R. Das, S. D. Bu, D. A. Felker, J. Lettieri, V. Vaithyanathan, S. S. N. Bharadwaja, N. Bassiri-Gharb, Y. B. Chen, H. P. Sun, C. M. Folkman, H. W. Jang, D. J. Kreft, S. K. Streiffer, R. Ramesh, X. Q. Pan, S. Trolhier-Mckinstry, D. G. Schlom, M. S. Rzchowski, R. H. Blick, C. B. Eom, *Science* **2011**, 334, 958.
- [15] S. K. Mishra, D. Pandey, A. P. Singh, *Appl. Phys. Lett.* **1996**, 69, 1707.
- [16] X. H. Du, J. Zheng, U. Belegundu, K. Uchino, *Appl. Phys. Lett.* **1998**, 72, 2421.
- [17] C. B. Yeager, Y. Ehara, N. Oshima, H. Funakubo, S. Trolhier-Mckinstry, *J. Appl. Phys.* **2014**, 116, 104907.
- [18] C. B. Yeager, S. Trolhier-Mckinstry, *J. Appl. Phys.* **2012**, 112, 074107.
- [19] N. Ledermann, P. Muralt, J. Paborowski, S. Gentil, K. Mukati, M. Cantoni, A. Seifert, N. Setter, *Sens. Actuators, A* **2003**, 105, 162.
- [20] R. A. Wolf, S. Trolhier-Mckinstry, *J. Appl. Phys.* **2004**, 95, 1397.
- [21] M. D. Nguyen, M. Dekkers, H. N. Vu, G. Rijnders, *Sens. Actuators, A* **2013**, 199, 98.
- [22] K. Tomioka, F. Kurokawa, R. Yokokawa, H. Kotera, K. Adachi, I. Kanno, *Jpn. J. Appl. Phys.* **2012**, 51, 09LA12.
- [23] S. Trolhier-Mckinstry, P. Muralt, *J. Electroceram.* **2004**, 12, 7.
- [24] D. Isarakorn, D. Briand, P. Janphuang, A. Sambri, S. Gariglio, J. M. Triscone, F. Guy, J. W. Reiner, C. H. Ahn, N. F. De Rooij, *Smart Mater. Struct.* **2011**, 20, 025015.
- [25] I. Kanno, *Jpn. J. Appl. Phys.* **2018**, 57, 040101.
- [26] J. S. Pulskamp, R. G. Polcawich, R. Q. Rudy, S. S. Bedair, R. M. Proie, T. Ivanov, G. L. Smith, *MRS Bull.* **2012**, 37, 1062.
- [27] I. Kanno, *J. Phys.: Conf. Ser.* **2015**, 660, 012001.
- [28] I. Kanno, H. Kotera, K. Wasa, T. Matsunaga, T. Kamada, R. Takayama, *J. Appl. Phys.* **2003**, 93, 4091.
- [29] M. Zhu, Z. Du, L. Jing, A. I. Yoong Tok, E. H. Tong Teo, *Appl. Phys. Lett.* **2015**, 107, 031907.
- [30] J. Ouyang, S. Y. Yang, L. Chen, R. Ramesh, A. L. Roytburd, *Appl. Phys. Lett.* **2004**, 85, 278.
- [31] Y. Tsujiura, S. Kawabe, F. Kurokawa, H. Hida, I. Kanno, *Jpn. J. Appl. Phys.* **2015**, 54, 10NA04.
- [32] G. Tan, K. Maruyama, Y. Kanamitsu, S. Nishioka, T. Ozaki, T. Umegaki, H. Hida, I. Kanno, *Sci. Rep.* **2019**, 9, 7309.
- [33] A. Sambri, D. Isarakorn, A. Torres-Pardo, S. Gariglio, P. Janphuang, D. Briand, O. Stéphan, J. W. Reiner, J. M. Triscone, N. F. de Rooij, C. H. Ahn, *Smart Mater. Res.* **2012**, 2012, 426048.
- [34] E.-J. Kim, S. H. Kweon, S. Nahm, Y. Sato, G. Tan, I. Kanno, *Appl. Phys. Lett.* **2022**, 121, 161901.
- [35] K. Saito, T. Kurosawa, T. Akai, T. Oikawa, H. Funakubo, *J. Appl. Phys.* **2003**, 93, 545.
- [36] K. Saito, T. Oikawa, I. Yamaji, T. Akai, H. Funakubo, *J. Cryst. Growth* **2002**, 237–239, 464.
- [37] Y. Ehara, S. Yasui, K. Ishii, H. Funakubo, *Jpn. J. Appl. Phys.* **2012**, 51, 09LA14.
- [38] S. K. Streiffer, C. B. Parker, A. E. Romanov, M. J. Lefevre, L. Zhao, J. S. Speck, W. Pompe, C. M. Foster, G. R. Bai, *J. Appl. Phys.* **1998**, 83, 2742.
- [39] H. Liu, P. Yang, K. Yao, J. Wang, *Appl. Phys. Lett.* **2010**, 96, 012901.
- [40] N. A. Pertsev, V. G. Kukhar, H. Kohlstedt, R. Waser, *Phys. Rev. B* **2003**, 67, 054107.
- [41] Y. Ehara, D. Ichinose, M. Kodera, T. Shiraishi, T. Shimizu, T. Yamada, K. Nishida, H. Funakubo, *Jpn. J. Appl. Phys.* **2021**, 60, SFFB07.
- [42] K. Morimoto, I. Kanno, K. Wasa, H. Kotera, *Sens. Actuators, A* **2010**, 163, 428.
- [43] H. G. Yeo, S. Trolhier-Mckinstry, *Sens. Actuators, A* **2018**, 273, 90.
- [44] S. Okamoto, T. Watanabe, K. Akiyama, S. Kaneko, H. Funakubo, S. Horita, *Jpn. J. Appl. Phys.* **2005**, 44, 5102.
- [45] K. Tokita, H. Hoshi, *Jpn. J. Appl. Phys.* **2000**, 39, 5399.